

Article

Influence of Nitride Coatings on Corrosion Resistance and the Biocompatibility of Titanium Alloy Products

Catherine Sotova ¹, Oleg Yanushevich ², Natella Krikheli ², Olga Kramar ², Alexey Vereschaka ^{3,*}, Semen Shehtman ^{1,2}, Filipp Milovich ⁴, Valery Zhyllinski ⁵, Anton Seleznev ² and Pavel Peretyagin ^{1,2}

- ¹ Department of High-Efficiency Machining Technologies, Moscow State University of Technology “STANKIN”, Vadkovsky Lane 3a, 127055 Moscow, Russia; e.sotova@stankin.ru (C.S.); s.shehtman@stankin.ru (S.S.); p.peretyagin@stankin.ru (P.P.)
- ² Scientific Department, Federal State Budgetary Educational Institution of Higher Education, “Russian University of Medicine” of the Ministry of Health of the Russian Federation, Dolgorukovskaya Str. 4, 127006 Moscow, Russia; mail@msmsu.ru (O.Y.); krikheli_ni@msmsu.ru (N.K.); dr.ovkramar@gmail.com (O.K.); a.seleznev@stankin.ru (A.S.)
- ³ Institute of Design and Technological Informatics of the Russian Academy of Sciences (IDTI RAS), Vadkovsky Lane 18a, 127055 Moscow, Russia
- ⁴ Department of Materials Science of Semiconductors and Dielectrics, National University of Science and Technology “MISiS”, Leninsky Prospect 4, 119049 Moscow, Russia; milovich.fo@misis.ru
- ⁵ Department of Chemistry, Technology of Electrochemical Production and Electronic Materials, Belarusian State Technological University, 13a, Sverdlov Street, 220006 Minsk, Belarus; zhyllinski@belstu.by
- * Correspondence: dra.veres@yandex.ru; Tel.: +7-9169100413

Abstract: The bioadhesion of bacteria to the surface of samples with Ti–TiN, Zr–ZrN, Zr–(Zr, Nb)N, and Zr–(Zr, Hf)N coatings was studied via incubation with gram-positive strains of *Staphylococcus aureus*. The samples were kept at 25 °C for 30 days in a 3% NaCl solution. The deposition of coatings slows, whereas oxidation processes intensify. The oxygen content on the TiN and (Zr, Nb)N coating surfaces was higher than that of the Ti sample without a coating. Samples with ZrN and, especially, (Zr, Hf)N coatings resist oxidation better. Regarding bioactivity toward *S. aureus*, the highest density of biological forms was observed on the surfaces of TiN and (Zr, Hf)N coatings. The lowest density was on the surfaces of uncoated, ZrN-coated, and (Zr, Nb)N-coated samples. On Ti–TiN, Zr–ZrN, and Zr–(Zr, Nb)N coatings, the formation of surface biostructures of a filamentary type was observed. In the uncoated sample, the biostructures have an island character, and in the sample with a Zr–(Zr, Hf)N coating, the formation of extensive areas of biostructures was observed. Between the biostructures and coating, a layer 5 to 15 nm thick was observed, presumably associated with bacterial adhesion. The presence of biostructures on the coating surface can activate or slow oxidation processes.

Keywords: bioadhesion; nitride coatings; corrosion resistance; biocompatibility; titanium alloy



Citation: Sotova, C.; Yanushevich, O.; Krikheli, N.; Kramar, O.; Vereschaka, A.; Shehtman, S.; Milovich, F.; Zhyllinski, V.; Seleznev, A.; Peretyagin, P. Influence of Nitride Coatings on Corrosion Resistance and the Biocompatibility of Titanium Alloy Products. *Metals* **2024**, *14*, 1200. <https://doi.org/10.3390/met14111200>

Academic Editor: Silvia Spriano

Received: 17 September 2024

Revised: 12 October 2024

Accepted: 16 October 2024

Published: 22 October 2024



Copyright: © 2024 by the authors. Licensee MDPI, Basel, Switzerland. This article is an open access article distributed under the terms and conditions of the Creative Commons Attribution (CC BY) license (<https://creativecommons.org/licenses/by/4.0/>).

1. Introduction

Biocompatibility is defined as the ability of an object to interact with biological systems without causing harm or undesirable reactions [1]. Nonetheless, one object can simultaneously interact with different biological systems, affecting them differently. For example, a medical implant simultaneously interacts with living tissues of the body and with pathogenic bacteria entering a wound. Accordingly, this object should be maximally biocompatible with the first system and, if possible, suppress the second system. When testing medical devices that function in the human body, the devices must have no or minimal toxic, allergic, or immunological reactions with respect to tissues or body fluids [2–5].

Among the materials used to produce implants and products functioning in the human body, titanium (Ti) alloys occupy an increasing market share due to their excellent biocompatibility, strength/specific gravity ratio, fatigue strength, and high anti-corrosion properties [1,6]. Of all Ti alloys, the most widely used at present is the Ti–6Al–4V alloy

(other designations, with a slight change in the range of element content, are VT6, TC4, Ti64, and ASTM Grade 5) [1,6–9]. This alloy is an α - β alloy with high strength and good corrosion resistance. In addition to Ti, this alloy contains about 6% aluminum (Al), 4% vanadium (V) (as a β -phase stabilizer), and a small amount of other alloy components, such as iron (Fe), zirconium (Zr), molybdenum (Mo), niobium (Nb), and tantalum (Ta) [10,11]. Despite the advantages of this material, the inclusion of V and Al creates problems due to their toxicity due to the leaching of free ions into the human body [1]. Thus, several studies [12,13] have demonstrated that V and Al in alloys have a toxic effect on biological objects and can lead to long-term health problems, such as neurological diseases and Alzheimer's disease [14–17]. Moreover, Al and Fe (although not toxic elements) lead to the formation of a connective tissue layer (fibrous tissue) around an implant and cause significant tissue contamination, a sign of insufficient bio-inertness of the metal [18,19].

Thus, several requirements, which are often difficult to combine, are imposed on the material of medical implants:

- High strength (primarily compression and bending), including fatigue strength;
- High corrosion resistance (including resistance to aggressive acidic and alkaline environments and electrolytic effects);
- Biocompatibility, implying biological inertness and the suppression of undesirable consequences (inflammatory processes, fibrous tissue formation, metallosis, etc.). Ideally, the implant material should prevent the attachment of harmful bacteria (i.e., prevent the formation of biofilm [20,21]) while promoting the attachment of protein and osteoblasts for successful osseointegration [22,23];
- Acceptable cost.

The Ti-6Al-4V alloy under consideration does not fully satisfy all these requirements. In addition to the undesirable and even dangerous effects of V and Al on the body, Ti is a very active element, and its inertness is due only to the fact that a strong TiO₂ film spontaneously forms on its surface, which is a barrier between the Ti substrate and environment. If this film is destroyed (e.g., via mechanical action, the influence of electrolytic processes, or the influence of acidic and alkaline environments), Ti begins to actively interact with environmental elements, which can lead to undesirable consequences.

An effective method to eliminate these problems and improve the performance properties of medical products comprising Ti alloys is applying special modifying coatings. Currently, coatings of various compositions and deposition methods are applied for this purpose, including the deposition of alkaline coatings using electrochemical, hydrothermal, or mixed processes [23]. These coatings create conditions for the better formation of reticular apatite and stimulation of bone tissue growth. The biphasic calcium phosphate (BCP)/TiO₂ coating obtained using the sol-gel method provides bioactivity, especially for bone tissue [24]. Deposition of Ta coatings on a Ti alloy substrate increases biocompatibility due to its noncytotoxicity in a physiological environment [25]. After applying a Ta coating, a six-fold higher osteoblast response was observed compared to an uncoated Ti substrate [26].

Recently, nitride coatings with various compositions have also been widely used for these purposes. The deposition of a TiN coating provides strong alkaline phosphatase activity with weak tartrate-resistant acid phosphatase activity [27]. The reduced presence of macrophages was observed at the implantation site. Implants with this coating have good biocompatibility and osseointegration.

The deposition of TiN and ZrN coatings improves biocompatibility, corrosion resistance, and degradation resistance [28]. This improvement has partly been confirmed by studies [29] in which products with TiN, ZrN, and DLC coatings demonstrated no inflammatory reactions or necrotic foci associated with the introduction of the implant. In addition, hemolysis tests assessing the chemical compatibility of coating samples with TiN and ZrN with blood exhibited no hemolytic activity. The genetic Ames test assessing mutagenic potential confirmed the clinical safety of all studied samples [30]. For all tested bacterial strains, the ZrN-coated sample displayed a higher percentage of dead bacteria

than other samples. A comparison of the properties of TiN- and ZrN-coated samples found higher cell colonization in the TiN-coated sample [31]. The deposition of the ZrN coating on the Ti-6Al-4V sample provided good corrosion resistance when exposed to saline, and it reduced the bioadhesion of *Staphylococcus aureus* bacteria [32].

Comparative studies of the anticorrosive properties of the Cr-CrN, Ti-TiN, Zr-ZrN, and Mo-MoN coatings [33] also found a noticeable advantage of the sample with the Zr-ZrN coating. Regarding the corrosion resistance of the TiN, ZrN, CrN/TiN, and CrN/ZrN coatings [34], samples with the ZrN and CrN/ZrN coatings demonstrated better corrosion resistance in a 3.5 wt.% sodium chloride (NaCl) solution and provided better biocompatibility and the efficient deposition of hydroxyapatite. An additional increase in the corrosion resistance of the ZrN/CrN coating is possible by increasing the number of binary layers in its structure [35]. The effectiveness of using multilayer CrN/TiN coatings to increase corrosion resistance was also confirmed [36]. A comparison of the corrosion resistance of the bilayer ZrN/CrN coating and monolayer CrN coating in a 3.5 wt.% NaCl solution found that the corrosion potential of the ZrN/CrN coating shifted higher and that the corrosion current density decreased compared to a single-layer CrN coating, a sign of better corrosion resistance [37]. Depositing Zr/ZrN and TiN/ZrN coatings noticeably increased corrosion resistance [38].

The properties of the Zr, ZrN, and ZrN/Zr coatings were investigated in simulated physiological environments [39], where the ZrN coating has the least tendency to corrode because additional energy is required to overcome the gap between the valence and conduction bands. The synergistic behavior in the ZrN/Zr bilayer offers a further increase in corrosion resistance.

A comparison of the anticorrosive properties of ZrN and tetrahedral amorphous carbon (ta-C) coatings [40] revealed that the ZrN-coated sample has better adhesion of the coating to the substrate and better corrosion resistance, microhardness, and wettability. However, the ta-C-coated sample provided better viability of *E. coli* and *S. aureus* cells.

The deposition of a (Zr, Si)N coating on a Ti alloy sample improved the albumin absorption and inhibited platelet adhesion. This result is beneficial in terms of improving the compatibility of the Ti implant with blood [41].

In addition, the NbN coating improved cell adhesion and the viability/proliferation of human cementoblasts [42]. A comparison of Nb-based coatings (NbO, NbC, and NbN) with Nb metal demonstrated significantly better corrosion resistance in potentiodynamic polarization and electrochemical impedance spectroscopy studies [43]. Further, the NbN coating improved cell adhesion, mineralization, and osteogenic differentiation. The TiN/NbN coating provided better corrosion resistance than the NbN and TiN coatings in a simulated body fluid environment [44]. The TiN/NbN coated sample surfaces demonstrated a significant reduction in bacterial count. Moreover, the bacterial count on the NbN coating surface was lower than on the TiN coating surface and uncoated substrate [44]. Human MDA-MB-231 cells adhered and proliferated well on the CrN/NbN coated surface, indicating good biocompatibility with this coating [45].

The coating based on HfN suppresses pathogenic microflora and has a bactericidal effect [46], and the (Hf, Si)N coating has good biocompatibility [47]. The number of platelets on the surface of the Ti alloy with the (Hf, Si)N coating is significantly lower than on that without a coating. On the surface without a coating, most platelets were activated, and pseudopodia in the form of branches appeared, some of which thickened and began to spread. In contrast, on the surface of the Ti alloy with the (Hf, Si)N coating, the platelets remained normal and round, without obvious pseudopodia of branches and agglomeration.

The ZrN-based coatings with Hf and Nb exhibited high corrosion resistance with high hardness and wear resistance [48]. Introducing Nb into the composition of ZrN slightly reduces corrosion resistance. In contrast, Hf increases the corrosion resistance. Carbonitride coatings of ZrCN and (Zr, Hf)CN have demonstrated good biocompatibility in vitro tests. After five days in a culture, osteosarcoma cells were well developed and had an ideal spindle-shaped form. Including Hf in the ZrCN coating composition allows for increased

corrosion resistance in Ringer's solution and improves biocompatibility [49]. It provides high cell viability, with dense and clearly defined actin bundles and strong contacts with the surface, favorable for the colonization of osteosarcoma cells on the surface of the (Zr, Hf)CN coating [49].

Thus, the objective of this work is to compare the biocompatibility and corrosion resistance of samples of the Ti alloy Ti–6Al–4V with nitride coatings with an adhesive sublayer based on pure metal. The Zr–ZrN coating, which has demonstrated high efficiency in numerous studies [28–39], is compared with coatings based on it with the introduction of Nb (Zr–(Zr, Nb)N) and Hf (Zr–(Zr, Hf)N). The object of comparison was a sample with a Ti–TiN coating, which also displayed high efficiency [27–29,31,33,34,36,44].

2. Materials and Methods

The coatings were deposited using the VIT-2 unit (IDTI RAS—MSUT “STANKIN”, Moscow, Russia), which has been described in detail in previous publications [50–54]. This study employs controlled accelerated arc physical vapor deposition technology [55,56]. This technology reduces the number of microparticles while maintaining a highly efficient deposition process and reducing energy costs. The Zr (99.98%) and Ti (99.99%) cathodes and Zr–Nb (50:50%) and Zr–Hf (50:50%) alloy cathodes were employed in this study. Before coating deposition, the samples were prepared as follows:

- By washing in a special solution at a temperature of 80 °C with ultrasonic stimulation;
- For washing, neutral detergent EKOSAN 400 (OOO TD “NOVA”, Moscow, Russia) was used. This detergent was chosen because it:
 - is biodegradable and safe for the environment
 - does not emit harmful substances
 - is fire- and explosion-proof
 - does not contain phosphates
- By rinsing in purified running water;
- By drying in a stream of hot, purified air.

During coating deposition, the arc currents of the Ti and Zr cathodes were 75 and 80 A, respectively. The arc currents of the Zr–Nb (50:50%) and Zr–Hf (50:50%) cathodes were 85 and 90 A, respectively. Other parameters were the same for all processes (nitrogen (N₂) pressure: 0.42 Pa, voltage on the substrate: –150 V, and tool rotation speed: 0.7 rpm).

The surface morphology and structure of the coatings were studied using a Carl Zeiss (Oberkochen, Germany) EVO 50 scanning electron microscope, with an energy dispersive X-ray (EDX) system X-Max with an active area of 80 mm² (Oxford Instruments, Abingdon, UK), and a transmission electron microscope (TEM) JEM 2100 (JEOL, Tokyo, Japan). The elemental composition was studied using TEM with EDX INCA Energy (Oxford Instruments, Abingdon, UK). The content of N and H were not determined because they are challenging to identify adequately using the methods in this work. These elements do not have a noticeable effect on oxidation processes and coating property degradation (unlike, e.g., oxygen, O). Samples for the TEM were prepared using a focused ion beam on a Strata 205 device (FEI Company, Hillsboro, OR, USA).

Corrosion Life Test Method in 3% NaCl with Preliminary Application of Microorganisms to the Coating Surface

The bioactivity of samples with Ti–TiN, Zr–ZrN, Zr–(Zr, Nb)N, and Zr–(Zr, Hf)N coatings was studied via incubation with gram-positive strains of *S. aureus* (American Type Culture Collection: ATCC 6538) [57,58]. Before the studies, the surface of the samples was sterilized in ethanol (70%) for 2 h and dried at room temperature under ultraviolet irradiation. Test bacteria (one colony) were transferred to a test tube with 2 mL of nutrient broth (NB), and the number of bacteria was determined. In accordance with the standards of the American Public Health Association and Association of Official Analytical Chemists International [59], the NB had the following composition (grams per liter of water): gelatin peptone of 5.0 g/L H₂O and meat extract of 3.0 g/L H₂O. The final pH was 6.8 ± 0.2 at

25 °C. The following method was used to prepare the NB: 8 g of the medium was diluted in 1 L of distilled water. Then, the solution was thoroughly mixed and heated. While stirring in a centrifuge, the solution was brought to a boil and boiled for a minute with rotation until completely dissolved. Then, the solution was poured into containers and sterilized for 15 min at 121 °C. The liquid with bacteria and NB was diluted so that the resulting solution contained 5.5×10^5 to 2.5×10^6 colony-forming units (CFU)/mL bacteria [58]. This solution was employed as a test liquid with bacteria. A volume of 0.1 mL of the liquid was inoculated onto the test sample, covered with a film, and lightly pressed so that the liquid was distributed over the entire surface [58]. The samples were placed in sterile polyethylene packages containing 50 mL of 3% NaCl solution and were kept at 25 °C for 30 days (720 h) (in accordance with GOST 9308 [60]).

3. Results

The presented map (Figure 1) of the element distribution on the surface of the Ti-6Al-4V alloy and TiN, (Zr, Hf)N, (Zr, Nb)N, and ZrN coatings after corrosion testing in a 3% NaCl solution at 25 °C for 720 h indicates the onset of oxidation processes and the formation of surface oxides. Although oxidation traces are present on all samples, the O distribution over the surface has significant differences. If the uncoated Ti substrate is characterized by the formation of spots 20 to 40 µm in size, then the TiN and (Zr, Nb)N coatings and, to a lesser extent, the ZrN coating are characterized by the formation of filiform structures of the mycelium type. The sample with the (Zr, Hf)N coating has extensive oxidation areas hundreds of microns long. The distribution of C, the second critical element that forms biological structures, was also examined to better understand the nature of the O-rich regions. The O and C concentration areas coincide in all samples, suggesting that the considered areas are of biological origin. The C intensity is significantly higher than the O intensity in the samples with the ZrN and (Zr, Hf)N coatings, whereas O dominates over C in the sample with the (Zr, Nb)N coating. This phenomenon may be associated with the intensity of the surface corrosion, coinciding with the development of biological forms. A higher O content, especially where C is absent or has low concentrations, may indicate surface oxidation without forming biological forms in these areas.

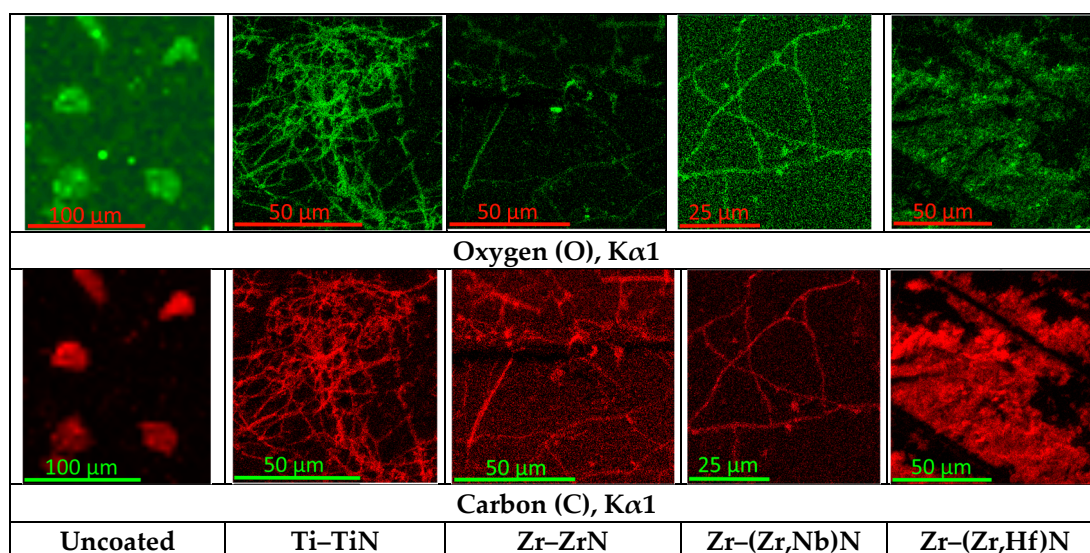


Figure 1. Mapping the distribution of oxygen and carbon (a marker of biological formations) on the surface of the studied coatings.

Some areas with high O/C content were examined in more detail to ensure that the considered areas were associated with forming biological forms. Moreover, the content of some other elements that are characteristic of biological forms was also considered (e.g., *S. aureus*; Figure 2).

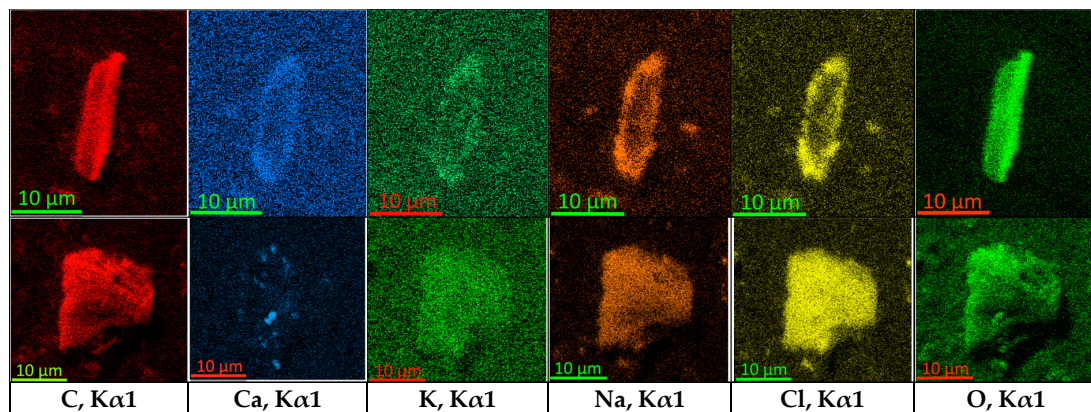


Figure 2. Analysis of the content of elements in the putative biological structures on the surface of the uncoated Ti-6Al-4V substrate, after corrosion tests in a 3% NaCl solution with preliminary planting of *Staphylococcus aureus*.

Table 1 lists the primary chemical elements comprising a typical prokaryotic cell (in this case, *E. coli*) [61,62]. Studies of the elemental composition of *S. aureus* have found similar elemental content values [63,64]. More than 90% of the elemental composition is C, hydrogen (H), O, N, phosphorus (P), and sulfur (S)—elements that form all biochemical substances and macromolecules comprising living systems [64]. In addition, this microorganism (in dry form) contains other trace elements, such as Fe, manganese (Mn), zinc (Zn), copper (Cu), and several others in small quantities. A comparison of the elemental composition of *E. coli* and the biological structures on the surface of the samples reveals that these compositions are close, especially for critical elements (C and O). Despite some content deviation in low-content elements, such as P, S, potassium (K), calcium (Ca) and others, the general elemental composition of the discovered formations corresponds to the bacteria composition; therefore, organic remains are observed rather than salt deposits.

Table 1. Elemental composition of *Escherichia coli* (wt./at.% in dry matter): (a) results, adapted from Refs. [61,62] and (b) results from the study of bioforms on samples.

	C	O	N	P	S	K	Na	Mg	Ca
wt.%	50.0	20.0	14.0	3.0	1.0	1.0	1.0	0.5	0.5
at.% (a)	63.21	20.22	15.17	1.71	0.47	0.68	0.68	0.31	0.35
wt.%	47.78–53.44	17.05–26.37	NA	2.75–11.24	1.08–2.57	2.25–4.13	1.80–2.10	0.24–0.72	1.7–8.81
at.% (b)	60.41–67.56	17.24–25.67	NA	1.57–6.41	0.51–1.21	1.53–2.81	1.23–1.41	0.15–0.45	1.19–6.17

After corrosion tests in a 3% NaCl solution, the more detailed maps of the element content on the uncoated Ti-6Al-4V substrate surface (Figure 2) facilitated analyzing the content of several elements that are characteristic of biological forms (i.e., *S. aureus*). The content of gases (N₂ and H₂) was not studied, but the content and intensity of the critical elements in Table 1 indicate that, as mentioned above, biological structures were observed rather than salt deposits, for example. The abnormally high content of Na and Cl in the studied areas is associated with the active deposition of NaCl crystals on the surface of biological formations. Obtaining data on the intensity of oxidation processes on the sample surfaces is possible after analyzing the average O content on the sample surfaces (Figure 3) and examining only areas with a low C content or without C (without biological forms). As established, the coating deposition can slow or intensify oxidation processes. The O content on the surface of the TiN and (Zr, Nb)N coatings is higher than that of the uncoated Ti sample. Samples with ZrN and, especially, (Zr, Hf)N coatings resist oxidation better in a 3% NaCl solution.

In terms of bioactivity toward *S. aureus*, the highest density of biological forms was observed on the surface of the TiN and (Zr, Hf)N coatings, and the lowest was on the surface of samples without a coating, with a ZrN coating, and with a (Zr, Nb)N coating (Figure 1). These results are consistent with past work [31,32,44] and confirm the decrease in

S. aureus adhesion in samples with the ZrN and (Zr, Nb)N coatings. Samples with the ZrN and (Zr, Hf)N coatings provide the best oxidation resistance. The O content in the surface layer of nitride coatings correlates with the results of corrosion tests (Table 2) conducted earlier [33,48]. The minimum corrosion currents in a 3% NaCl solution were observed for samples with Zr–ZrN ($0.123 \mu\text{A}/\text{cm}^2$), compared to the uncoated Ti–6Al–4V alloy ($0.372 \mu\text{A}/\text{cm}^2$). The introduction of Hf into ZrN allowed reducing the corrosion currents from $0.123 \mu\text{A}/\text{cm}^2$ (Zr–ZrN coating) to $0.118 \mu\text{A}/\text{cm}^2$ (Zr–(Zr, Hf)N coating) [33,48], which is consistent with the decrease in the O content in the coating from 4.09 to 1.01 wt.%. The Zr–(Zr, Nb)N and Ti–TiN coatings are characterized by corrosion currents of 0.395 and $0.411 \mu\text{A}/\text{cm}^2$ [33,48], corresponding to 6.92 and 6.89 at.%, respectively, of O in the coatings after 262 h in a 3% NaCl solution at 25 °C.

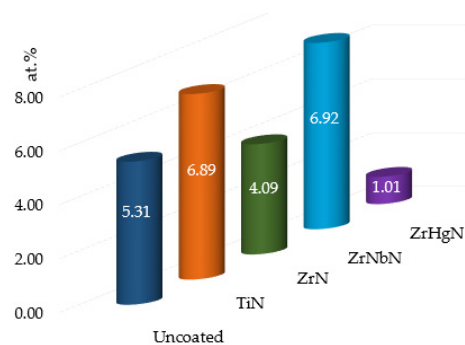


Figure 3. Comparison of the average oxygen content (at.%) on the surface of the studied samples with various coatings.

Impedance studies of nitride coating corrosion in a 3% NaCl solution at 25 °C [47] have also found a degree of surface oxidation after 262 h of corrosion in 3% NaCl at 25 °C. A maximum R^2 value (charge transfer resistance) of $2.36 \text{ MOhm}\cdot\text{cm}^2$ was observed for Ti–6Al–4V samples with a Zr–(Zr, Hf)N coating, for which the minimum O content of 1.01 at.% was observed. This finding indicates the formation of a pore-free oxide film on the surface of the Zr–(Zr, Hf)N coating, preventing the corrosion process in a 3% NaCl solution at 25 °C.

Table 2. Resource corrosion tests of Ti–6Al–4V samples with nitride coatings in 3% NaCl at 25 °C.

No	Coating	Corrosion Current Density [33], $\mu\text{A}/\text{cm}^2$	R^2 (Charge Transfer Resistance) [47], $\text{MOhm}\cdot\text{cm}^2$	Surface Oxidation after 262 H in 3% NaCl at 25 °C, wt.% O
1	Uncoated	0.372	-	5.31 ± 0.71
2	Zr–(Zr, Nb)N	0.395	1.10	6.92 ± 0.46
3	Zr–(Zr, Hf)N	0.118	2.36	1.01 ± 0.19
4	Zr–ZrN	0.123	0.06	4.09 ± 0.24
5	Ti–TiN	0.411	-	6.89 ± 0.57

The nature of the formation of biostructures and oxidation processes on the sample surfaces with coatings is considered in more detail below.

3.1. TiN Coating

The Ti–TiN coating exhibits the formation of surface biostructures of a filamentary type (Figure 4a). These structures are presumably the remains of filamentous colonies of *S. aureus*. The localization crossing this thread was selected for cutting out the lamella. The study of the lamella (Figure 4b) revealed a characteristic columnar structure of TiN, which maintains strong adhesion to the substrate. A thin film (about 15 nm thick) was observed on the coating surface, presumably representing the remains of the NaCl solution (accurate analysis of the composition is difficult due to the slight thickness). A section of the remains of the surface biological structure (Figure 4c) indicates the presence of internal cavities (bubbles). A film with a thickness of about 11 nm occurs between the biostructure

and coating surface. This film is different from the film on the free surface of the coating. The thickness of the film is slightly lower, and it is lighter in contrast. In addition, cavities (delaminations from the substrate) were observed in its structure. Due to the minimal thickness of this film, a more detailed study is challenging. This film is assumed to promote the adhesion of *S. aureus* to the coating surface [65,66]. Bacterial adhesion to material surfaces is a complex process influenced by the physicochemical properties of the cells and the substrate surface. It has been established that *S. aureus* can attach to hydrophobic and hydrophilic surfaces, with the former having higher adhesion [66]. In addition, studies have found that *S. aureus* has high adhesion to the surfaces of products that directly contact humans and, thus, can penetrate and infect the body [67]. Accordingly, reducing the adhesion of *S. aureus* is a critical task.

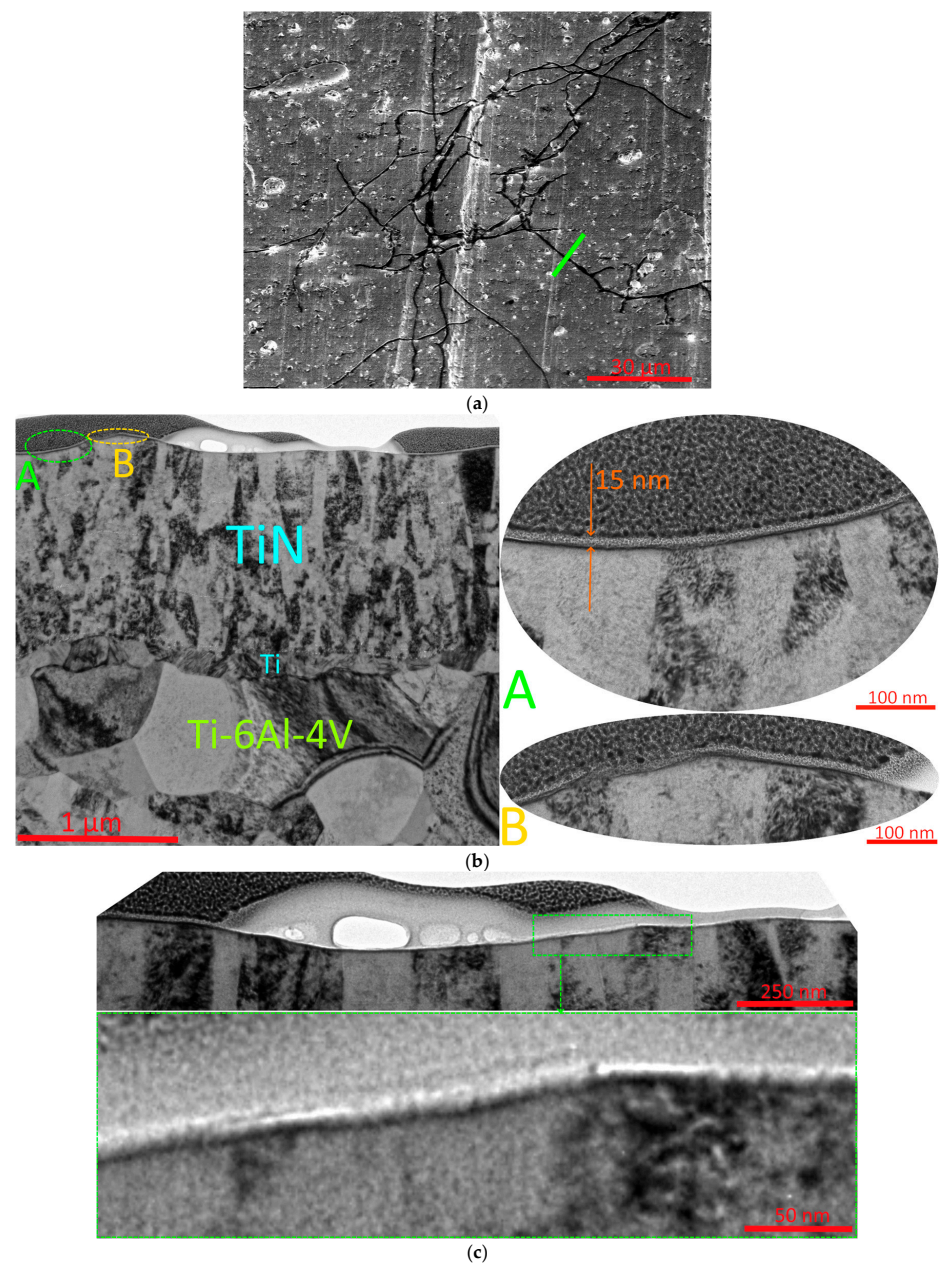


Figure 4. Structure of the Ti-TiN coating on Ti-6Al-4V alloy after corrosion testing in a 3% NaCl solution at 25 °C for 720 h: (a) view of the sample surface, where the green line indicates the location of the lamella cutout, (b) general view of the lamella across the coating thickness, and (c) biostructure and its adhesion to the coating.

The study of the elemental composition of the interfacial area of the Ti–TiN coating and biostructure indicates a fairly high O content (up to 9.85 at.%; Figure 5a). The analysis of the elemental composition of the biostructure did not provide meaningful results, exhibiting a dominant C content with some O content (up to 5.66 at.%; Figure 5b). This result may be associated with the partial destruction of the initial biostructure during the cutting of the lamella (charring and decomposition of organic compounds).

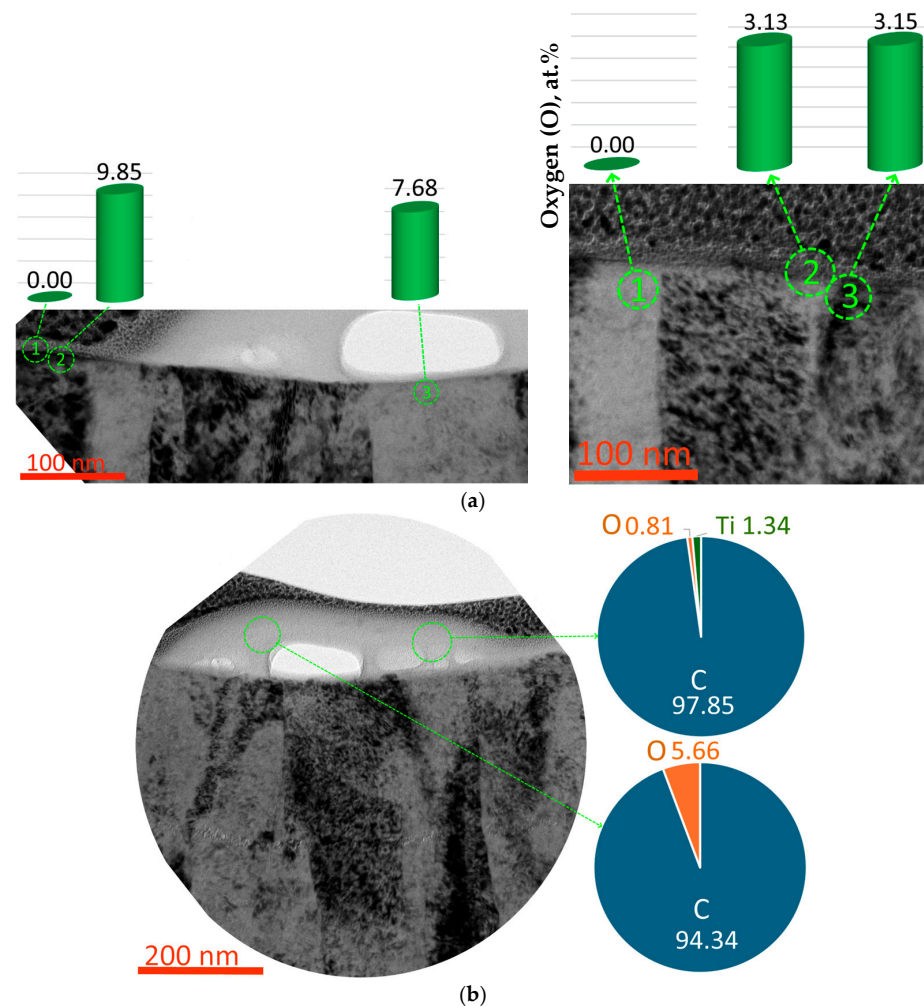


Figure 5. Distribution of elements in the surface layers of the Ti–TiN coating on Ti–6Al–4V alloy at the boundary with the biological structure after corrosion tests in a 3% NaCl solution at 25 °C for 720 h: (a) oxygen content in the coating surface layers and (b) analysis of the elemental composition of the biostructure.

3.2. ZrN Coating

After corrosion tests in a 3% NaCl solution, a network of filiform structures similar to the Ti–TiN coating was observed on the surface of the Zr–ZrN coating (Figure 6a). The total concentration of these biostructures on the surface of the Zr–ZrN coating is significantly lower. The analysis of the coating structure (Figure 6b) indicates the presence of columnar grains and the preservation of tight adhesion to the substrate (Ti–6Al–4V). A section of the biostructure was observed on the coating surface with no cavities (bubbles). The contrast of the coating structure image under the biostructure is somewhat lighter than that of the free area of the coating.

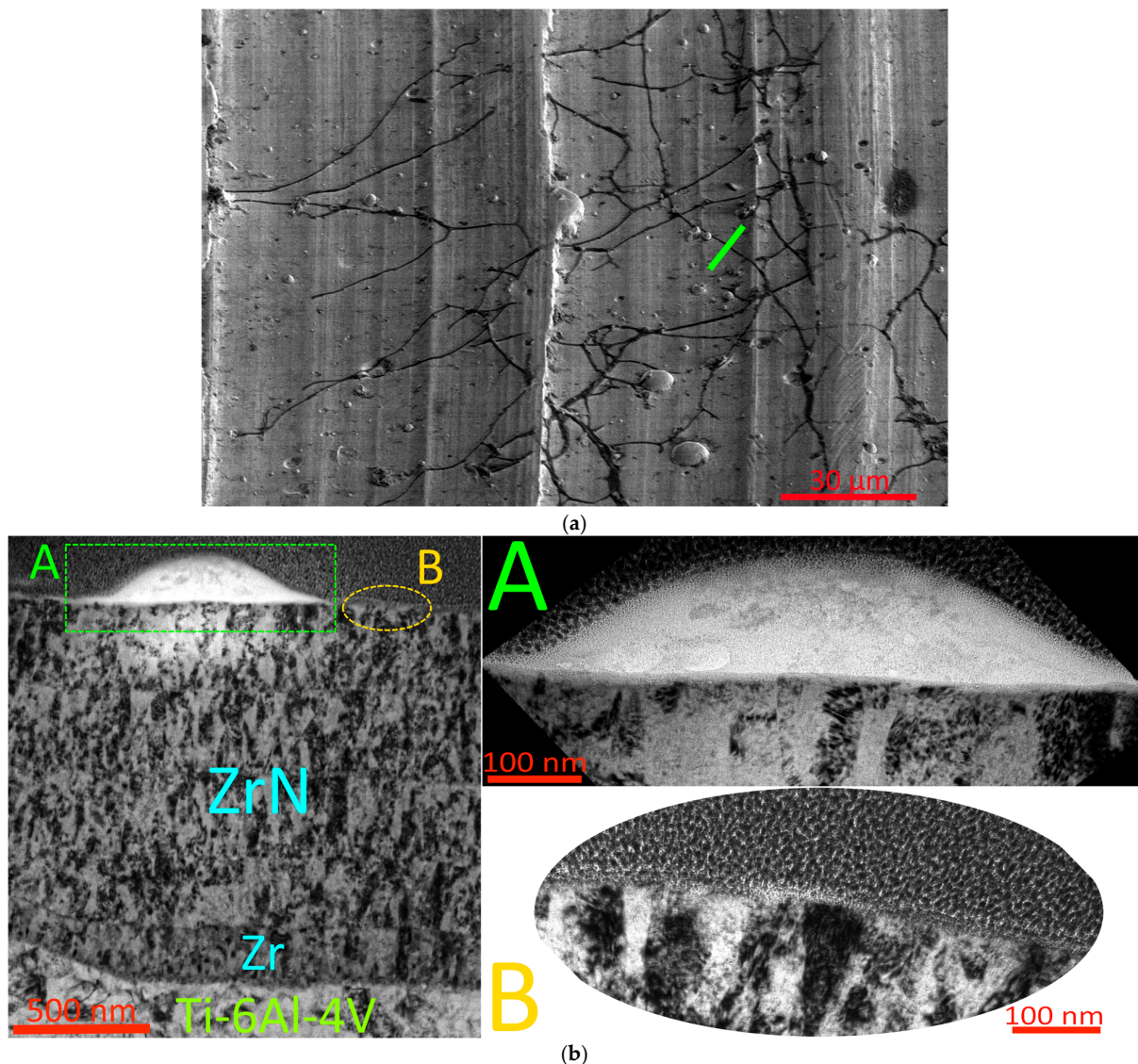


Figure 6. Structure of the Zr–ZrN coating on Ti–6Al–4V alloy after corrosion testing in a 3% NaCl solution at 25 °C for 720 h: (a) view of the sample surface, where the green line indicates the location of the lamella cutout and (b) the structure of the coating and biostructure on its surface.

A study of the O distribution in the coating surface layers revealed that the presence of this element in the coating (and, consequently, the coating oxidation) is uneven (Figure 7a). Along with zones in which a relatively high (up to 7.1 at.%) O presence was observed, O is practically absent in some zones.

The study of the elemental composition of the biostructure on the coating surface provides an interesting result (Figure 7b). The content of the chemical elements in this zone correlates well with the described bacteria composition [61–64] (Table 1). Thus, the studied biostructure is precisely formed by *S. aureus* with a high degree of certainty. Directly under the adhesion area of the biostructure with the coating is an area with an abnormally high O content of 13.13 at.% (a lighter contrast area in Figure 7c). Up to 6.75 at.% of O is retained at a depth of up to 700 nm, whereas O is absent at a depth of 100 nm in the layers under the free surface of the coating, and the O content is not recorded at all measurement points even on the surface (Figure 7a). Such intense local oxidation is associated with the effect of this biostructure. Oxygen may be a product of the chemical interaction of the coating components and biostructure and might diffuse deep into the coating. The cause and nature of this effect are to be assessed in further work.

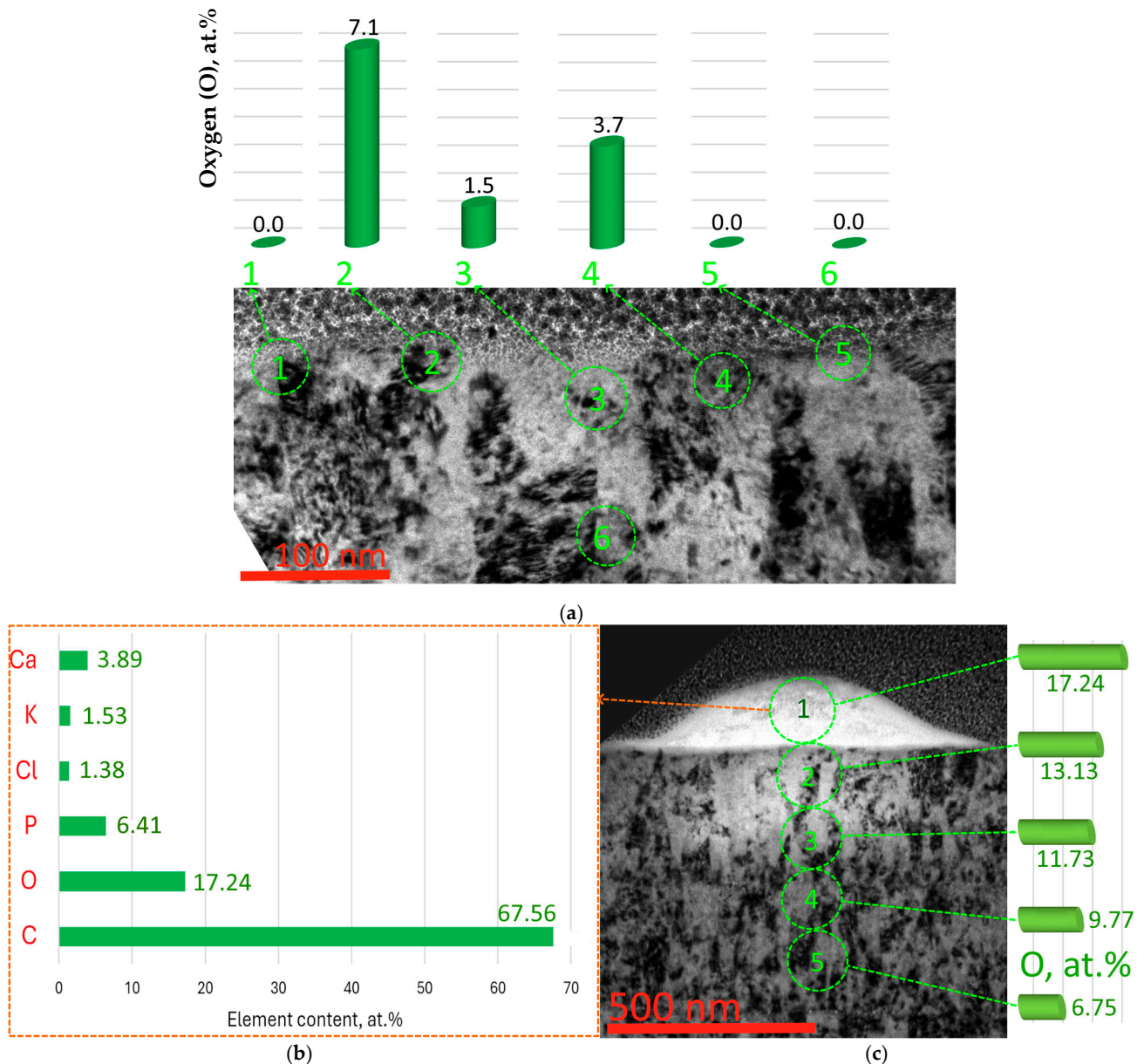


Figure 7. Oxygen (O) content in the surface layers of the Zr–ZrN coating on Ti–6Al–4V alloy after corrosion testing in 3% NaCl at 25 °C for 720 h: (a) O content in the coating surface layer, (b) study of the elemental composition of the biostructure, and (c) O content across the coating thickness in the area under the biostructure.

3.3. Zr–(Zr,Nb)N Coating

The filamentary biostructures on the surface of the Zr–(Zr, Nb)N coating are less pronounced than the previously studied coatings (Figure 8a). Cavities (bubbles) measuring 10 to 40 nm were visible on the cross section of the biostructure (Figure 8b). A very thin (about 5 nm) layer (Figure 8c) was observed between the coating and biostructure, indicating the interaction of the biostructure with the coating. It is not possible to differentiate the elemental composition of this layer from the general elemental composition of the biostructure.

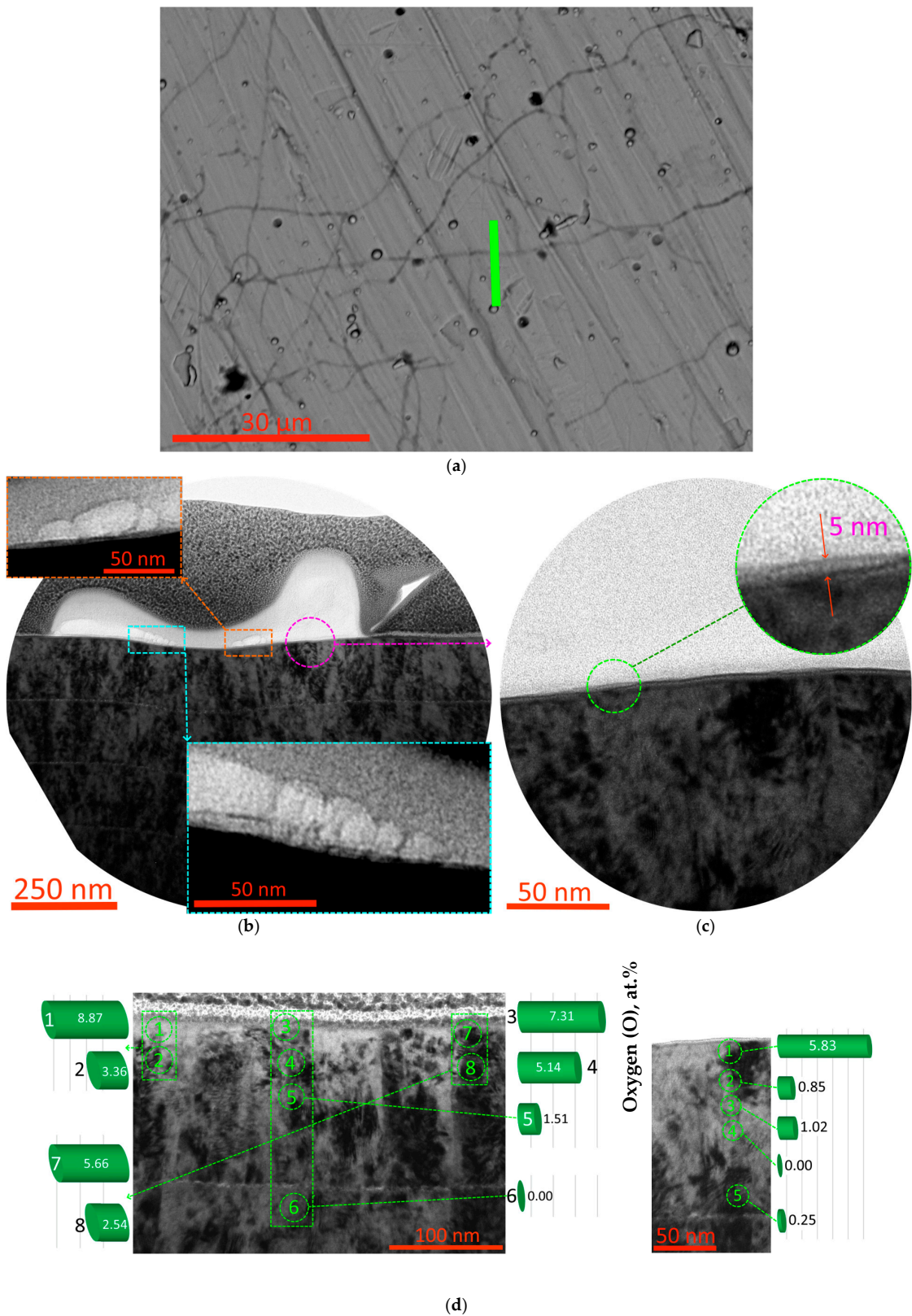


Figure 8. (a) Surface of the Zr-(Zr, Nb)N coating with filiform biostructures and the location of the lamella cut out (green line). (b) Section and structure of the biostructure on the coating surface. (c) Structure of the intermediate layer between the biostructure and coating. (d) Distribution of oxygen by the depth of the Zr-(Zr, Nb)N coating on Ti-6Al-4V alloy after corrosion testing in a 3% NaCl solution at 25 °C for 720 h.

The analysis of the O distribution in the surface and deep layers of the coating indicates a high degree of oxidation. The surface layers have up to 8.87 at.% of O, and there is still 1.51 at.% of O at a depth of 200 nm (Figure 8d). Oxidation occurs to a depth of at least 200 nm, which may indicate a uniform dissolution of the Zr-(Zr, Nb)N coating, acting as a protective layer (this effect is described in [33,47]). Due to its gradual destruction, the attachment of the biostructure is difficult (the distribution density of the biostructure “threads” on the surface is significantly lower than that of other samples; Figure 8a).

3.4. Zr-(Zr, Hf)N Coating

The surface of the Zr-(Zr, Hf)N coating after corrosion tests in a 3% NaCl solution displays significant differences from the coatings discussed above. In this case, the formation of filiform biostructures was not observed, but continuous areas of biostructures with a width of 30 to 50 μm and an extension of hundreds of μm were present (Figure 9a). The cross section of this biostructure reveals that its thickness ranges from 20 to 200 nm (Figure 9b). The elemental composition of the biostructure typically corresponds to those discussed earlier and indicates a possible relationship with *S. aureus* (Figure 9c).

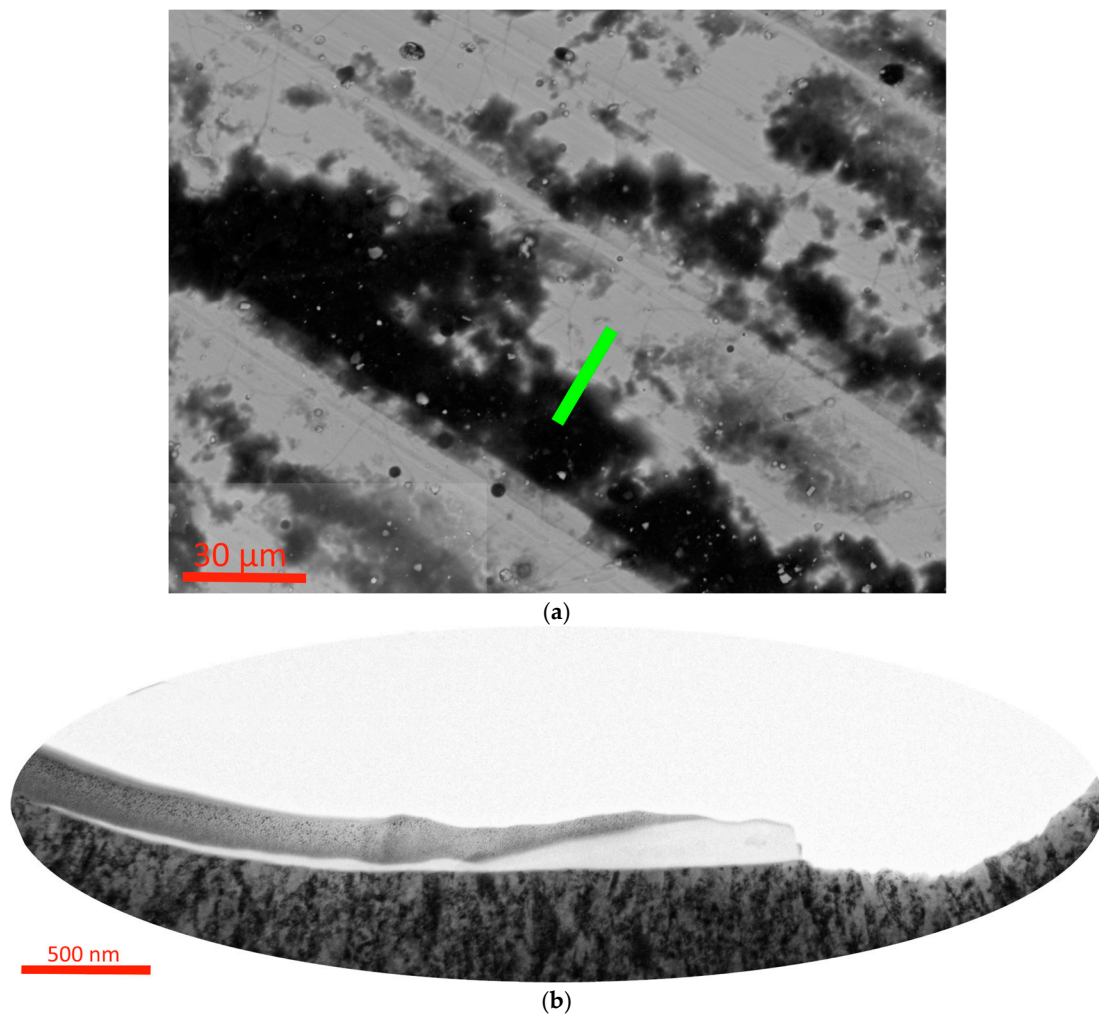


Figure 9. Cont.

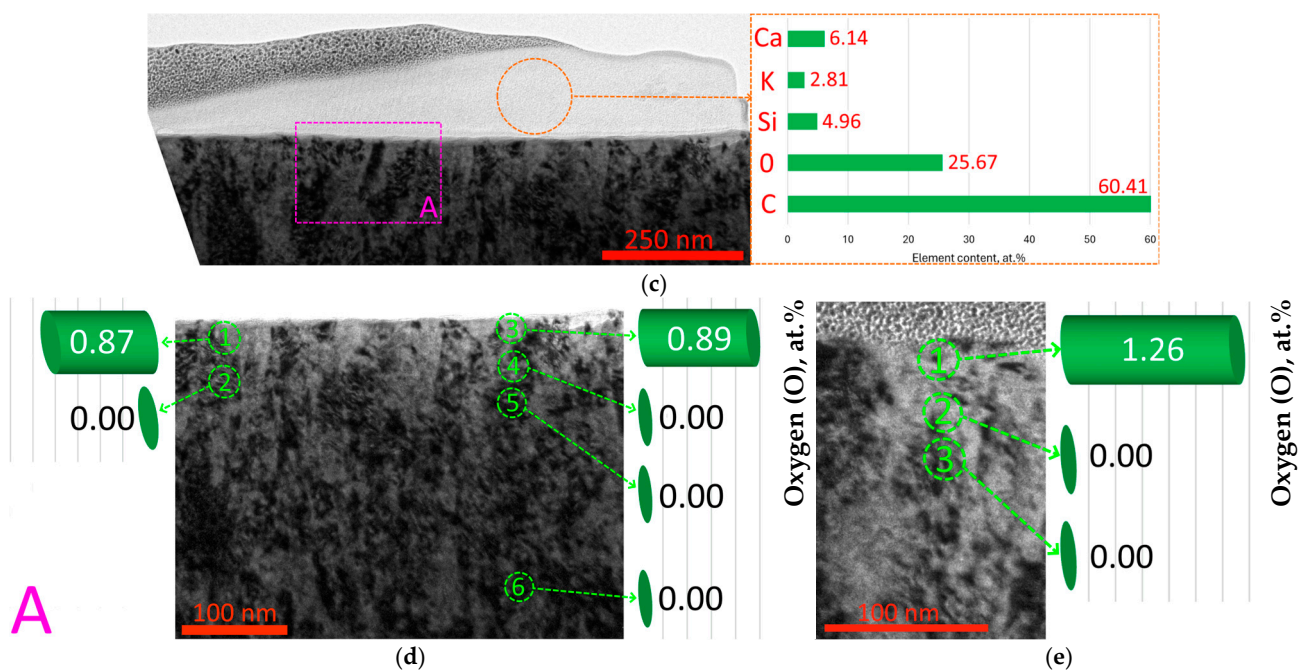


Figure 9. (a) Surface of the Zr-(Zr, Hf)N coating with biostructures and the location of the lamella cut out (green line). (b) Section and structure of the biostructure on the coating surface. (c) Elemental and phase composition of the biostructure. (d) Distribution of oxygen by the depth of the Zr-(Zr, Hf)N coating on Ti-6Al-4V alloy after corrosion testing in a 3% NaCl solution at 25 °C for 720 h in region A under the biostructure and (e) under the free surface of the coating.

This coating displayed an extremely low tendency to oxidation. Even in the surface layer, the O content does not exceed 1.26 at.%. These results correlate well with the results of previously conducted electrochemical studies [33,47]. The O content in the coating under the biostructure (0.87 to 0.89 at.%) is even slightly lower than on the free surface of the coating (1.26 at.%). Thus, active oxidation associated with the influence of the biostructure (as in the sample with the Zr-ZrN coating; Figure 7b) is not observed, which may indicate a sufficient density of the biostructure film, blocking the access of O in the coating.

4. Conclusions

The adherence (bioadhesion) of bacteria to the surface of coated samples was studied via incubation with gram-positive strains of *S. aureus*. The samples were kept at 25 °C for 30 days in a 3% NaCl solution. Based on the study results, the following conclusions were drawn:

- Coating deposition can slow and intensify oxidation processes. The O content on the surface of the TiN and (Zr, Nb)N coatings is higher than that of the uncoated Ti sample. Samples with ZrN and, especially, (Zr, Hf)N coatings resist oxidation better.
- In terms of bioactivity with respect to *S. aureus*, the highest density of biological forms was observed on the surface of the TiN and (Zr, Hf)N coatings, and the lowest was on the surface of uncoated samples and those with a ZrN or (Zr, Nb)N coating.
- On Ti-TiN, Zr-ZrN, and Zr-(Zr, Nb)N coatings, the formation of surface biostructures of a filamentary type was observed. These structures are presumably the remains of filamentary colonies of *S. aureus*. In this case, the uncoated sample has an island-like biostructure, whereas the sample with the Zr-(Zr, Hf)N coating reveals the formation of extensive biostructure areas.
- A 5 to 15 nm thick layer was observed between the biostructure and TiN and Zr-(Zr, Nb)N coatings, presumably representing the products of chemical interactions of the biostructure with the coating components, affecting the adhesive interaction of *S. aureus* with the sample surfaces.

- An area of active oxidation to a depth of 700 nm was observed under the biostructure on the Zr–ZrN coating, whereas in the sample with the Zr–(Zr, Hf)N coating, the O content under the biostructure is lower than on the free surface of the coating. This phenomenon may be associated with the peculiarities of the chemical interaction of the biostructure and coating material, requiring additional research.

Thus, the presence of biostructures on the surface of the coated samples can activate or slow oxidation processes, depending on the coating composition. Based on the obtained data, the Zr–ZrN coating has the best application prospects among the coatings under consideration.

Author Contributions: Conceptualization, C.S. and A.V.; methodology, C.S., A.V., O.Y. and P.P.; resources P.P.; investigation, F.M., A.S., N.K., O.K., F.M. and A.S.; data curation, C.S., A.V., O.Y. and V.Z.; writing—original draft preparation, C.S., A.V. and V.Z.; writing—review and editing, C.S., A.V., S.S. and V.Z.; project administration, A.V. and P.P.; funding acquisition, P.P. All authors have read and agreed to the published version of the manuscript.

Funding: This work was supported by the Ministry of Health of the Russian Federation under project 056-00041-23-00.

Data Availability Statement: The original contributions presented in the study are included in the article, further inquiries can be directed to the corresponding author.

Acknowledgments: The study used the equipment from the Centre for collective use of Moscow State University of Technology “STANKIN” (agreement No. 075-15-2021-695, 26 July 2021).

Conflicts of Interest: The authors declare no conflict of interest.

References

1. Bandyopadhyay, A.; Mitra, I.; Goodman, S.B.; Kumar, M.; Bose, S. Improving biocompatibility for next generation of metallic implants. *Prog. Mater. Sci.* **2023**, *133*, 101053. [[CrossRef](#)] [[PubMed](#)]
2. Williams, D.F. On the mechanisms of biocompatibility. *Biomaterials* **2008**, *29*, 2941–2953. [[CrossRef](#)] [[PubMed](#)]
3. Todros, S.; Todesco, M.; Bagnò, A. Biomaterials and their biomedical applications: From replacement to regeneration. *Processes* **2021**, *9*, 1949. [[CrossRef](#)]
4. Malik, N.A.; Sant, P.; Ajmal, T.; Ur-Rehman, M. Implantable antennas for biomedical applications. *IEEE J. Electromagn. RF Microw. Med. Biol.* **2020**, *5*, 84–96. [[CrossRef](#)]
5. Zare, M.; Ghomi, E.R.; Venkatraman, P.D.; Ramakrishna, S. Silicone-based biomaterials for biomedical applications: Antimicrobial strategies and 3D printing technologies. *J. Appl. Polym. Sci.* **2021**, *138*, 50969. [[CrossRef](#)]
6. Lütjering, G.; Williams, J.C. *Titanium*; Springer Science & Business Media: Berlin/Heidelberg, Germany, 2007.
7. Pesode, P.; Barve, S. A review—Metastable β titanium alloy for biomedical applications. *J. Eng. Appl. Sci.* **2023**, *70*, 25. [[CrossRef](#)]
8. Aufa, A.N.; Hassan, M.Z.; Ismail, Z. Recent advances in Ti-6Al-4V additively manufactured by selective laser melting for biomedical implants: Prospect development. *J. Alloys Compd.* **2022**, *896*, 163072. [[CrossRef](#)]
9. Mohan Agarwal, K.; Singhal, A.; Kapoor, A.; Bhatia, D. Simulated analysis of Ti-6Al 4V processed through equal channel angular pressing for biomedical applications. *Mater. Sci. Energy Technol.* **2021**, *4*, 290–295. [[CrossRef](#)]
10. Gautam, S.; Bhatnagar, D.; Bansal, D.; Batra, H.; Goyal, N. Recent advancements in nanomaterials for biomedical implants. *Biomed. Eng. Adv.* **2022**, *3*, 100029. [[CrossRef](#)]
11. Stavinoha, J.N. *Investigation of Plasma Arc Welding as a Method for the Additive Manufacturing of Ti-6Al-4V Alloy Components*; Montana Tech of the University of Montana: Butte, MT, USA, 2012.
12. Steinemann, S.G.; Perren, S.M. Titanium alloys as metallic biomaterials. In Proceedings of the Fifth World Conference on Titanium, Munich, Germany, 10–14 September 1984; Volume 2, pp. 1327–1334.
13. Sidelnikov, A.I. Comparative characteristics of materials of the titanium group used in the production of modern dental implants. *InfoDENT* **2000**, *5*, 10–12.
14. Mirza, A.; King, A.; Troakes, C.; Exley, C. Aluminium in brain tissue in familial Alzheimer’s disease. *J. Trace Elem. Med. Biol.* **2017**, *40*, 30–36. [[CrossRef](#)] [[PubMed](#)]
15. Cremasco, A.; Messias, A.D.; Esposito, A.R.; Duek, E.A.R.; Caram, R. Effects of alloying elements on the cytotoxic response of titanium alloys. *Mat. Sci. Eng. C* **2011**, *31*, 833–839. [[CrossRef](#)]
16. Lin, C.-W.; Ju, C.-P.; Lin, J.-H.C. A comparison of the fatigue behavior of cast Ti-7.5Mo with c.p. titanium, Ti-6Al-4V and Ti-13Nb-13Zr alloys. *Biomaterials* **2005**, *26*, 2899–2907. [[CrossRef](#)] [[PubMed](#)]

17. Cardoso, G.C.; de Almeida, G.S.; Corrêa, D.O.G.; Zambuzzi, W.F.; Buzalaf, M.A.R.; Correa, D.R.N.; Grandini, C.R. Preparation and characterization of novel as-cast Ti-Mo-Nb alloys for biomedical applications. *Sci. Rep.* **2022**, *12*, 11874. [[CrossRef](#)]
18. Zhang, L.-C.; Chen, L.-Y. A review on biomedical titanium alloys: Recent progress and prospect. *Adv. Eng. Mater.* **2019**, *21*, 1801215. [[CrossRef](#)]
19. Sotova, C.; Yanushevich, O.; Kriheli, N.; Grigoriev, S.; Evdokimov, V.; Kramar, O.; Nozdrina, M.; Peretyagin, N.; Undritsova, N.; Popelyshkin, E.; et al. Dental Implants: Modern Materials and Methods of Their Surface Modification. *Materials* **2023**, *16*, 7383. [[CrossRef](#)]
20. Donlan, R.M.; Costerton, J.W. Biofilms: Survival mechanisms of clinically relevant microorganisms. *Clin. Microbiol. Rev.* **2002**, *15*, 147–148. [[CrossRef](#)]
21. Hook, A.L.; Chang, C.-Y.; Yang, J.; Luckett, J.; Cockayne, A.; Atkinson, S.; Mei, Y.; Bayston, R.; Irvine, D.J.; Langer, R.; et al. Combinatorial discovery of polymers resistant to bacterial attachment. *Nat. Biotechnol.* **2012**, *30*, 868. [[CrossRef](#)]
22. Zhao, L.; Chu, P.K.; Zhang, Y.; Wu, Z. Antibacterial Coatings on Titanium Implants. *J. Biomed. Mater. Res. B* **2009**, *91*, 470–480. [[CrossRef](#)]
23. Takematsu, E.; Katsumata, K.; Okada, K.; Niinomi, M.; Matsushita, N. Bioactive surface modification of Ti–29Nb–13Ta–4.6 Zr alloy through alkali solution treatments. *Mater. Sci. Eng. C* **2016**, *62*, 662–667. [[CrossRef](#)]
24. Dikici, B.; Niinomi, M.; Topuz, M.; Koc, S.G.; Nakai, M. Synthesis of biphasic calcium phosphate (BCP) coatings on beta-type titanium alloys reinforced with rutile-TiO₂ compounds: Adhesion resistance and in-vitro corrosion. *J. Sol-Gel Sci. Technol.* **2018**, *87*, 713–724. [[CrossRef](#)]
25. Black, J. Biologic performance of tantalum. *Clin. Mater.* **1994**, *16*, 167–173. [[CrossRef](#)] [[PubMed](#)]
26. Balla, V.K.; Banerjee, S.; Bose, S.; Bandyopadhyay, A. Direct laser processing of a tantalum coating on titanium for bone replacement structures. *Acta Biomater.* **2010**, *6*, 2329–2334. [[CrossRef](#)] [[PubMed](#)]
27. Sovak, G.; Weiss, A.; Gotman, I. Osseointegration of Ti6Al4V alloy implants coated with titanium nitride by a new method. *J. Bone Joint Surg. Br.* **2000**, *82*, 290–296. [[CrossRef](#)]
28. Taran, A.V.; Garkusha, I.E.; Taran, V.S.; Pyvovar, N.V.; Muratov, R.M.; Leonovych, A.V.; Nikolaychuk, G.P.; Baturin, A.A. Structure of biocompatible nanocoatings obtained by physical vapor deposition on flexible polyurethane for medical applications. *J. Adv. Microsc. Res.* **2018**, *13*, 313–319. [[CrossRef](#)]
29. Hajduga, M.B.; Bobinski, R. TiN, ZrN and DLC nanocoatings—A comparison of the effects on animals, in-vivo study. *Mater. Sci. Eng. C* **2019**, *104*, 109949. [[CrossRef](#)]
30. Brunello, G.; Brun, P.; Gardin, C.; Ferroni, L.; Bressan, E.; Meneghello, R.; Zavan, B.; Sivolella, S. Biocompatibility and antibacterial properties of zirconium nitride coating on titanium abutments: An in vitro study. *PLoS ONE* **2018**, *13*, e0199591. [[CrossRef](#)]
31. Prachar, P.; Bartakova, S.; Brezina, V.; Cvrcek, L.; Vanek, J. Cytocompatibility of implants coated with titanium nitride and zirconium nitride. *Bratisl. Med. J.* **2015**, *116*, 154–156. [[CrossRef](#)]
32. Ramoul, C.; Beliardouh, N.E.; Bahi, R.; Nouveau, C.; Djahoudi, A.; Walock, M.J. Surface performances of PVD ZrN coatings in biological environments. *Tribology—Mater. Surf. Interfaces* **2019**, *13*, 12–19. [[CrossRef](#)]
33. Tao, H.; Zhyllinski, V.; Vereschaka, A.; Chayeuski, V.; Yuanming, H.; Milovich, F.; Sotova, C.; Seleznev, A.; Salychits, O. Comparison of the Mechanical Properties and Corrosion Resistance of the Cr–CrN, Ti–TiN, Zr–ZrN, and Mo–MoN Coatings. *Coatings* **2023**, *13*, 750. [[CrossRef](#)]
34. Noori, M.; Atapour, M.; Ashrafzadeh, F.; Elmkhah, H.; di Configno, G.G.; Ferraris, S.; Perero, S.; Cardu, M.; Spriano, S. Nanostructured multilayer CAE-PVD coatings based on transition metal nitrides on Ti6Al4V alloy for biomedical applications. *Ceram. Int.* **2023**, *49*, 23367–23382. [[CrossRef](#)]
35. Samim, P.M.; Fattah-alhosseini, A.; Elmkhah, H.; Imantalab, O. Nanoscale architecture of ZrN/CrN coatings: Microstructure, composition, mechanical properties and electrochemical behavior. *J. Mater. Res. Technol.* **2021**, *15*, 542–560. [[CrossRef](#)]
36. Fazel, Z.A.; Elmkhah, H.; Fattah-Alhosseini, A.; Babaei, K.; Meghdari, M. Comparing electrochemical behavior of applied CrN/TiN nanoscale multilayer and TiN singlelayer coatings deposited by CAE-PVD method. *J. Asian Ceram. Soc.* **2020**, *8*, 510–518. [[CrossRef](#)]
37. Samim, P.M.; Fattah-alhosseini, A.; Elmkhah, H.; Imantalab, O.; Nouri, M. A study on comparing surface characterization and electrochemical properties of single-layer CrN coating with nanostructured multilayer ZrN/CrN coating in 3.5 wt.% NaCl solution. *Surf. Interfaces* **2020**, *21*, 100721. [[CrossRef](#)]
38. Vladescu, A.; Kiss, A.; Braic, M.; Cotrut, C.M.; Drob, P.; Balaceanu, M.; Vasilescu, C.; Braic, V. Vacuum arc deposition of nanostructured multilayer coatings for biomedical applications. *J. Nanosci. Nanotechnol.* **2008**, *8*, 733–738. [[CrossRef](#)]
39. Zambrano, D.F.; Hernández-Bravo, R.; Ruden, A.; Espinosa-Arbelaez, D.G.; González-Carmona, J.M.; Mujica, V. Mechanical, tribological and electrochemical behavior of Zr-based ceramic thin films for dental implants. *Ceram. Int.* **2023**, *49*, 2102–2114. [[CrossRef](#)]
40. Aslan, N.; Aksakal, B.; Cihangir, S.; Cetin, F.; Yilmazer, Y. ZrN and ta-C coatings on titanium for biomedical applications: Improved adhesion, corrosion, antibacterial activity, and cytotoxicity properties. *J. Mater. Res.* **2023**, *38*, 3923–3936. [[CrossRef](#)]
41. Cui, X.; Jin, G.; Hao, J.; Li, J.; Guo, T. The influences of Si content on biocompatibility and corrosion resistance of Zr-Si-N films. *Surf. Coat. Technol.* **2013**, *228* (Suppl. S1), S524–S528. [[CrossRef](#)]

42. Ramírez, G.; Rodil, S.E.; Arzate, H.; Muhl, S.; Olaya, J.J. Niobium based coatings for dental implants. *Appl. Surf. Sci.* **2011**, *257*, 2555–2559. [[CrossRef](#)]
43. Xu, Z.; Yate, L.; Qiu, Y.; Aperador, W.; Coy, E.; Jiang, B.; Moya, S.; Wang, G.; Pan, H. Potential of niobium-based thin films as a protective and osteogenic coating for dental implants: The role of the nonmetal elements. *Mater. Sci. Eng. C* **2019**, *96*, 166–175. [[CrossRef](#)]
44. Subramanian, B. Enhancement of biocompatibility of metal implants by nanoscale TiN/NbN multilayer coatings. *J. Nanosci. Nanotechnol.* **2013**, *13*, 4565–4572. [[CrossRef](#)] [[PubMed](#)]
45. Huang, W.; Zalnezhad, E.; Musharavati, F.; Jahanshahi, P. Investigation of the tribological and biomechanical properties of CrAlTiN and CrN/NbN coatings on SST 304. *Ceram. Int.* **2017**, *43*, 7992–8003. [[CrossRef](#)]
46. Abdullin, I.S.; Mironov, M.M.; Garipova, G.I. Bactericidal and biologically stable coatings for medical implants and instruments. *Med. Tekh.* **2004**, *4*, 20–22.
47. Cui, X.; Hao, J.; Wang, Y.; Dong, M.; Jin, G. The effect of Si content on the performance of magnetron sputtering Hf-Si-N films. *Phys. Procedia* **2013**, *50*, 427–432. [[CrossRef](#)]
48. He, T.; Zhylinski, V.; Vereschaka, A.; Keshin, A.; Huo, Y.; Milovich, F.; Sotova, C.; Seleznev, A. Influence of niobium and hafnium doping on the wear and corrosion resistance of coatings based on ZrN. *J. Mater. Res. Technol.* **2023**, *27*, 6386–6399. [[CrossRef](#)]
49. Cotrut, C.-M.; Braic, V.; Balaceanu, M.; Titorencu, I.; Braic, M.; Parau, A.C. Corrosion resistance, mechanical properties and biocompatibility of Hf-containing ZrCN coatings. *Thin Solid Films* **2013**, *538*, 48–55. [[CrossRef](#)]
50. Vereschaka, A.A.; Bublikov, J.I.; Sitnikov, N.N.; Oganyan, G.V.; Sotova, C.S. Influence of nanolayer thickness on the performance properties of multilayer composite nano-structured modified coatings for metal-cutting tools. *Int. J. Adv. Manuf. Technol.* **2018**, *95*, 2625–2640. [[CrossRef](#)]
51. Grigoriev, S.; Vereschaka, A.; Milovich, F.; Migranov, M.; Andreev, N.; Bublikov, J.; Sitnikov, N.; Oganyan, G. Investigation of the tribological properties of Ti-TiN-(Ti,Al,Nb,Zr)N composite coating and its efficiency in increasing wear resistance of metal cutting tools. *Tribol. Int.* **2021**, *164*, 107236. [[CrossRef](#)]
52. Vereschaka, A.; Grigoriev, S.; Milovich, F.; Sitnikov, N.; Migranov, M.; Andreev, N.; Bublikov, J.; Sotova, C. Investigation of tribological and functional properties of Cr,Mo-(Cr,Mo)N-(Cr,Mo,Al)N multilayer composite coating. *Tribol. Int.* **2021**, *155*, 106804. [[CrossRef](#)]
53. Vereschaka, A.; Milovich, F.; Andreev, N.; Seleznev, A.; Alexandrov, I.; Muranov, A.; Mikhailov, M.; Tatarkanov, A. Comparison of properties of ZrHf-(Zr,Hf)N-(Zr,Hf,Cr,Mo,Al)N and Ti-TiN-(Ti,Cr,Al)N nanostructured multilayer coatings and cutting properties of tools with these coatings during turning of nickel alloy. *J. Manuf. Processes* **2023**, *88*, 184–201. [[CrossRef](#)]
54. Grigoriev, S.; Vereschaka, A.; Zelenkov, V.; Sitnikov, N.; Bublikov, J.; Milovich, F.; Andreev, N.; Sotova, C. Investigation of the influence of the features of the deposition process on the structural features of microparticles in PVD coatings. *Vacuum* **2022**, *202*, 111144. [[CrossRef](#)]
55. Grigoriev, S.; Vereschaka, A.; Milovich, F.; Sitnikov, N.; Seleznev, A.; Sotova, C.; Bublikov, J. Influence of the yttrium cathode arc current on the yttrium content in the (Ti,Y,Al)N coating and the coating properties. *Vacuum* **2024**, *222*, 113028. [[CrossRef](#)]
56. Grigoriev, S.N.; Volosova, M.A.; Fedorov, S.V.; Migranov, M.S.; Mosyanov, M.; Gusev, A.; Okunkova, A.A. The Effectiveness of Diamond-like Carbon a-C:H:Si Coatings in Increasing the Cutting Capability of Radius End Mills When Machining Heat-Resistant Nickel Alloys. *Coatings* **2022**, *12*, 206. [[CrossRef](#)]
57. *Staphylococcus aureus* subsp. *aureus* Rosenbach. Available online: <https://www.atcc.org/products/6538> (accessed on 2 August 2024).
58. Pyanko, A.V.; Sergievich, D.S.; Chernik, A.A.; Makarova, I.V.; Kharitonov, D.S.; Makeeva, I.S. Physicochemical and biocidal properties of nickel-TiN and nickel-TiN-titania coatings. *Prot. Met. Phys. Chem. Surf.* **2021**, *57*, 88–95. [[CrossRef](#)]
59. AOAC International. *Official Methods of Analysis*, 22nd ed.; AOAC International: Rockville, MD, USA, 2023.
60. GOST 9.308-85 (Russia). Unified System of Protection against Corrosion and Aging. Metallic and Non-Metallic Inorganic Coatings. Methods of Accelerated Corrosion Tests. Available online: <https://internet-law.ru/gosts/gost/20202/> (accessed on 2 August 2024).
61. Hamadi, F.; Latrache, H.; Zahir, H.; El Abed, S.; Ellouali, M.; Saad, I.K. The Relation Between the Surface Chemical Composition of Escherichia coli and their Electron Donor/Electron Acceptor (Acid-base) Properties. *Res. J. Microbiol.* **2012**, *7*, 32–40. [[CrossRef](#)]
62. Kenneth, T. The Good, the Bad, and the Deadly: Online Textbook of Bacteriology; Bacteria and Archaea and the Cycles of Elements in the Environment (Page 1). Available online: https://www.academia.edu/download/48563182/Todars_Online_Textbook_of_Bacteriology.pdf (accessed on 30 August 2024).
63. Seltmann, G.; Beer, W. Chemical composition of the capsule material of *Staphylococcus aureus* strain 1193/74. *Z. Allg. Mikrobiol.* **1976**, *16*, 445–452.
64. Christian, J.H.B.; Waltho, J.A. The Composition of *Staphylococcus aureus* in Relation to the Water Activity of the Growth Medium. *J. Gen. Microbiol.* **1964**, *35*, 205–213. [[CrossRef](#)]
65. Hamadi, F.; Latrache, H.; Mabrouki, M.; Elghmari, A.; Outzourhit, A.; Ellouali, M.; Chtaini, A. Effect of pH on distribution and adhesion of *Staphylococcus aureus* to glass. *J. Adhes. Sci. Technol.* **2005**, *19*, 73–85. [[CrossRef](#)]

66. Zmantar, T.; Bettaieb, F.; Chaieb, K.; Ezzili, B.; Mora-Ponsonnet, L.; Othmane, A.; Jaffrézic, N.; Bakhrouf, A. Atomic force microscopy and hydrodynamic characterization of the adhesion of *Staphylococcus aureus* to hydrophilic and hydrophobic substrata at different pH values. *World J. Microbiol. Biotechnol.* **2011**, *27*, 887–896. [[CrossRef](#)]
67. Azelmad, K.; Hamadi, F.; Mimouni, R.; Amzil, K.; Latrache, H.; Mabrouki, M.; El Boulani, A. Adhesion of *Staphylococcus aureus* and *Staphylococcus xylosum* to materials commonly found in catering and domestic kitchens. *Food Control* **2017**, *73*, 156–163. [[CrossRef](#)]

Disclaimer/Publisher’s Note: The statements, opinions and data contained in all publications are solely those of the individual author(s) and contributor(s) and not of MDPI and/or the editor(s). MDPI and/or the editor(s) disclaim responsibility for any injury to people or property resulting from any ideas, methods, instructions or products referred to in the content.